chemistry proceedings

MDPI

Proceeding Paper

Leveraging Cross-Family Catalytic Conservation for Structure-Based Virtual Screening of *Leishmania* Phospholipid Cyclopropane Fatty Acid Synthases †

Juan Diego Guarimata [1,*], José R. Mora [2] and Martin Lavecchia [1]

[1] Centro de Química Inorgánica "Dr. Pedro J. Aymonino", CEQUINOR (UNLP, CCT-CONICET La Plata, Associated with CIC-PBA), Departamento de Química, Facultad de Ciencias Exactas, Universidad Nacional de La Plata, Boulevard 120 N 1465, La Plata CP1900, Argentina; lavecchia@quimica.unlp.edu.ar

[2] Grupo de Química Computacional y Teórica (QCT-USFQ), Departamento de Ingeniería Química, Universidad San Francisco de Quito, Quito 170901, Ecuador; jrmora@usfq.edu.ec

* Correspondence: juanguarimata@quimica.unlp.edu.ar

† Presented at the 30th International Electronic Conference on Synthetic Organic Chemistry, 5–19 November 2026; https://sciforum.net/event/ecsoc-30/home.

Abstract

Cyclopropane fatty acid (CFA) synthases are S-adenosylmethionine-dependent enzymes that remodel microbial membrane lipids but remain an overlooked class of antiparasitic targets. In *Leishmania* spp., the phospholipid CFA synthases govern membrane composition, cell shape, and stress resistance. Because fatty acid cyclopropanation has no human counterpart, this enzyme represents an intrinsically parasite-selective target. Combining sequence analysis with cross-family structural superposition, we show that the catalytic machinery of *Leishmania* CFA synthases is conserved across both subgroups of the family: the monomeric mycobacterial mycolic-acid synthases (e.g., CmaA1) and the bacterial phospholipid CFA synthases from *Escherichia coli*, *Aquifex aeolicus*, and *Lactobacillus acidophilus*. Structure-based virtual screening of a library of 98,294 lipophilic compounds against CmaA1 (PDB 1KPH), followed by docking into modeled *L. infantum* and *L. mexicana* CFA synthases, 200 ns molecular dynamics simulations and MM-PBSA binding free-energy calculations, identified several chemotypes, including an 8,16-pyranthrenedione scaffold, that bound both parasite enzymes and formed stable complexes. Although these scaffolds are predominantly lipophilic, this physicochemical profile is consistent with the membrane-associated nature of the target. Rather than identifying a single privileged scaffold, these findings indicate that the conserved CFA synthase active site can accommodate multiple chemically distinct ligands, supporting the enzyme family as a tractable, parasite-selective target class and a promising basis for synergistic, multi-target antileishmanial therapies.

Keywords: *Leishmania*; cyclopropane fatty acid synthase; molecular docking; molecular dynamics; virtual screening; drug discovery

Check for updates

Academic Editor: Julio A. Seijas

Published: 15 October 2026

Copyright: © 2026 by the authors. Licensee MDPI, Basel, Switzerland. This article is an open access article distributed under the terms and conditions of the Creative Commons Attribution (CC BY) license.

1. Introduction

Fatty acid cyclopropanation is a specialized lipid modification catalyzed by S-adenosylmethionine (SAM)-dependent cyclopropane fatty acid (CFA) synthases, found mainly in microorganisms [1]. It adds a cyclopropane ring across lipid double bonds, increasing membrane rigidity and favoring resistance to environmental and host-induced stress [1]. In *Mycobacterium tuberculosis*, CmaA1 cyclopropanates mycolic acids and is linked to virulence, immune evasion and drug resistance [2,3]. *Leishmania* spp. possess

phospholipid CFA synthases of probable bacterial origin that, although they cyclopropanate membrane phospholipids rather than mycolic acids, retain a CmaA1-like catalytic mechanism and govern membrane composition, cell shape and acid-stress resistance, properties tied to parasite survival within the host [4,5]. Because fatty acid cyclopropanation has no human counterpart, CFA synthases are an intrinsically parasite-selective target class.

Structurally, the family comprises two subgroups: the monomeric mycobacterial enzymes that cyclopropanate mycolic acids, built on a single Class I methyltransferase domain and typified by CmaA1 [6], and the bi-domain bacterial enzymes that act on membrane phospholipids, characterized for *Escherichia coli* [7], *Lactobacillus acidophilus* [8] and *Aquifex aeolicus* [1]. The catalytic domain and the active-site bicarbonate coordination are conserved across the whole family. By origin and predicted architecture, the *Leishmania* enzymes belong to the bacterial phospholipid-synthase subgroup rather than to the mycobacterial mycolic-acid type; that shared catalytic core nonetheless justifies CmaA1 as the structural reference. Rather than advocating any single chemotype, this work puts the phospholipid CFA synthase family forward as an attractive, largely unexploited target class for leishmaniasis and applies a structure-based virtual screening to deliver structurally validated chemical starting points.

2. Materials and Methods

2.1. Ligand Retrieval and Preparation

SMILES strings for 98,294 lipophilic compounds (logP > 5) were retrieved from the ZINC20 database (https://zinc.docking.org/, accessed on 22 January 2026) [9]. Three-dimensional structures and conformers were generated with OMEGA v5.0.0.3 in "pose" mode, which produces conformer ensembles for the OEDocking suite [10]. The co-crystallized ligand of CmaA1 (didecyl dimethyl ammonium, DDDMAB) was extracted from PDB 1KPH and prepared with the same protocol, serving as the structural reference ligand for the active-site pocket throughout docking.

2.2. Target Preparation and Structural Analysis

M. tuberculosis mycolic acid cyclopropane synthase (CmaA1) was obtained from the RCSB Protein Data Bank (https://www.rcsb.org/, accessed on 23 January 2026), accession code 1KPH [6]. In the absence of experimental structures, *Leishmania* CFA synthases were retrieved for *L. infantum* and *L. mexicana* from the AlphaFold Protein Structure Database (https://alphafold.ebi.ac.uk/, accessed on 23 January 2026) [11], using the NCBI reference sequences (https://www.ncbi.nlm.nih.gov/, accessed on 23 January 2026) XP_001463394.1 (*L. infantum*) and XP_003872617.1 (*L. mexicana*). Conservation of key residues was assessed by sequence alignment against CmaA1 with the MultAlin server (http://multalin.toulouse.inra.fr/multalin/, accessed on 23 January 2026) and ESPript (https://espript.ibcp.fr/ESPript/ESPript/index.php, accessed on 23 January 2026) [12,13]. A cross-family structural superposition was then built in UCSF Chimera v1.19 [14], overlaying CmaA1 (1KPH), representative of the monomeric mycobacterial subgroup, with the bacterial phospholipid CFA synthases of *Escherichia coli* (6BQC), *Lactobacillus acidophilus* (5Z9O) and *Aquifex aeolicus* (7QOS), together with the two *Leishmania* models. Protein–ligand complexes and interaction diagrams were generated and visualized with BIOVIA Discovery Studio Visualizer v25.1.0.24284 (Dassault Systèmes, San Diego, CA, USA) [15].

2.3. Molecular Docking

Receptors were prepared with Make Receptor v4.3.0.3 (OpenEye Scientific Software, Santa Fe, NM, USA) [16]. For each target, the docking box was centered on the SAM/substrate binding pocket and manually adjusted to enclose the whole catalytic cavity,

and the site shape potential was generated with default outer and inner contours, keeping cofactors. The resulting receptor files were saved in the OEB format for docking with FRED. Docking of all compounds and the reference ligand DDDMAB (1.053 Å RMSD on redocking) was performed on CmaA1 with FRED v4.3.0.3 (OEDocking suite) [16]. Because the CmaA1 and *Leishmania* CFA synthase active sites are highly conserved, this first screen on the experimentally characterized CmaA1 served as a pre-filter, and the top-ranked 2865 compounds were redocked against the *L. infantum* and *L. mexicana* CFA synthases, testing up to four conformers per compound together with DDDMAB.

2.4. Molecular Dynamics Simulations

Lead complexes were simulated for 200 ns in GROMACS 2019 [17]. Ligand topologies were generated with the General Amber Force Field through ACPYPE [18] and input files were prepared with Open Babel [19]; CmaA1 (1KPH) was pre-processed in UCSF Chimera, removing the native ligand, crystallographic waters and hydrogens. Each complex was embedded in a cubic TIP3P box with a 1.2 nm solute-to-edge clearance (box edges of about 8.3 nm for CmaA1 and 10.5–10.9 nm for the *Leishmania* systems; ~17,000–40,000 water molecules) and neutralized with counter-ions (6 Na^+ for CmaA1, 4 Cl^- for *L. infantum* and 4 Na^+ for *L. mexicana*). Systems were energy-minimized by steepest descent and equilibrated in two 100 ps phases (NVT then NPT) before production under Parrinello–Rahman pressure coupling (1 bar) and a Berendsen thermostat (300 K), with hydrogen-bond lengths constrained by LINCS to allow a 2 fs time step.

2.5. Binding Free Energy Calculations

Binding free energies were estimated with the Molecular Mechanics Poisson–Boltzmann Surface Area (MM-PBSA) method as implemented in g_mmpbsa [20]; the polar term was obtained from the Poisson–Boltzmann equation and the non-polar term from the solvent-accessible surface area, computed every 5 ns between 10 and 200 ns. The configurational entropy term ($-T\Delta S$) was not included, so the reported values represent the enthalpic (effective) contribution and are used for relative ranking.

3. Results and Discussion

Sequence and structural analysis (Figure 1) showed that CmaA1 and the modeled *L. infantum* and *L. mexicana* CFA synthases conserve the SAM-binding site, the hydrophobic lipid pocket and the catalytic environment. Tyr33, Cys35, Gly137 and Glu140 (CmaA1 numbering, used throughout) are conserved [6]: Tyr33 is proposed to stabilize the carbocationic intermediate through a cation–π interaction, while Cys35 and the Glu140 carboxylate coordinate a bicarbonate ion that abstracts the methyl proton and relays it to that carboxylate, the terminal base [21]. The presence of Gly137, replaced by glutamate in oxygenating homologs, supports specialization in cyclopropanation [6]. Superposition with experimentally solved representatives of both subgroups confirmed that the catalytic pocket is preserved family-wide (Figure 1c).

Mapping these conserved positions onto the models shows that the *Leishmania* CFA synthase active site reproduces the bipartite architecture of CmaA1 [22]: a cofactor-binding site that accommodates SAM/SAH and an adjacent hydrophobic channel that houses the long unsaturated acyl chain of the substrate. Within this arrangement, the conserved Tyr33 lines the catalytic pocket and is oriented to stabilize the carbocationic intermediate, while the Cys35/Glu140-coordinated bicarbonate ion is ideally placed to abstract the methyl proton and close the cyclopropane ring (Figure 1b) [21]. A deep hydrophobic sub-pocket (Tyr232, Ile169, Phe200) provides the apolar environment that orients the unsaturated fatty acyl chain. Because this organization is preserved from the mycobacterial enzyme to the

parasite models, the catalytic and substrate-binding determinants exploited for inhibitor design in CmaA1 are also available in *Leishmania* CFA synthases.

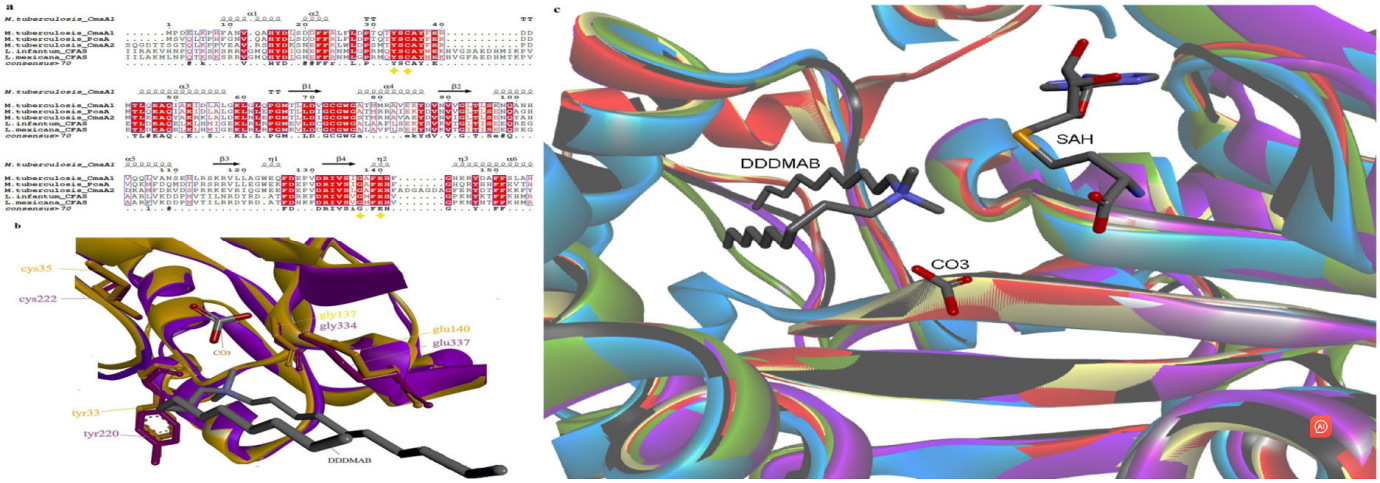


Figure 1. Sequence and structural comparison of CmaA1 and *Leishmania* CFA synthases. (**a**) Sequence alignment using CmaA1 as reference (CCP46213.1); key residues (Tyr33, Cys35, Gly137, Glu140) are marked. (**b**) Structural alignment of CmaA1 (yellow) and *L. infantum* CFA synthase (purple) around the catalytic and bicarbonate-coordinating environment. (**c**) Active-site superposition of both subgroups, CmaA1 (blue), *Escherichia coli* (black), *Aquifex aeolicus* (green) and *Lactobacillus acidophilus* (purple), overlaid with the modeled *L. infantum* (red) and *L. mexicana* (yellow) CFA synthases.

Docking of the full library against CmaA1 (Table 1) ranked highly lipophilic compounds (logP 6–10) at the top, consistent with a hydrophobic, lipid-binding pocket. Next, the molecular docking of the top hits from the previous process against the *Leishmania* CFA synthases (Table 2) identified several chemotypes binding both enzymes more strongly than DDDMAB. Molecule **1** (ZINC33753889) and molecule **2** (ZINC111871939), which share an 8,16-pyranthrenedione scaffold (Figure 2), ranked among the best in CmaA1 and in both parasite enzymes, indicating cross-affinity toward conserved sites. Interaction analysis (Figure 3) showed both molecules occupying the catalytic pocket; in molecule **2,** the bromine points toward the solvent and makes no active-site contacts, marking it as a site for optimization.

Table 1. Best docking hits against CmaA1, ranked by FRED Chemgauss4 score.

ZINC20 ID	MW (g/mol)	logP (ZINC20)	FRED Score
ZINC33753889	509.78	8.75	−21.35
ZINC111871939	554.23	8.86	−20.58
ZINC223708003	722.02	9.84	−20.42
ZINC584578353	530.10	6.16	−20.38
ZINC100396879	501.84	9.52	−20.30
ZINC100102745	502.53	7.69	−20.27
DDDMAB (ref.)	326.38	9.30	−14.87

Table 2. Top hits against *L. infantum* and *L. mexicana* CFA synthases (FRED Chemgauss4 score).

***L. infantum* CFA Synthase**		***L. mexicana* CFA Synthase**	
ZINC20 ID	**FRED Score**	**ZINC20 ID**	**FRED Score**
ZINC33753889	−15.49	ZINC33753889	−15.24
ZINC141594793	−15.12	ZINC223708003	−14.74

Table 2. *Cont.*

L. infantum CFA Synthase		*L. mexicana* CFA Synthase	
ZINC20 ID	**FRED Score**	**ZINC20 ID**	**FRED Score**
ZINC111871939	−14.62	ZINC111871939	−14.72
ZINC223708003	−14.15	ZINC141594793	−14.43
ZINC22073802	−14.15	ZINC1920075	−14.10
DDDMAB (ref.)	−10.48	DDDMAB (ref.)	−10.49

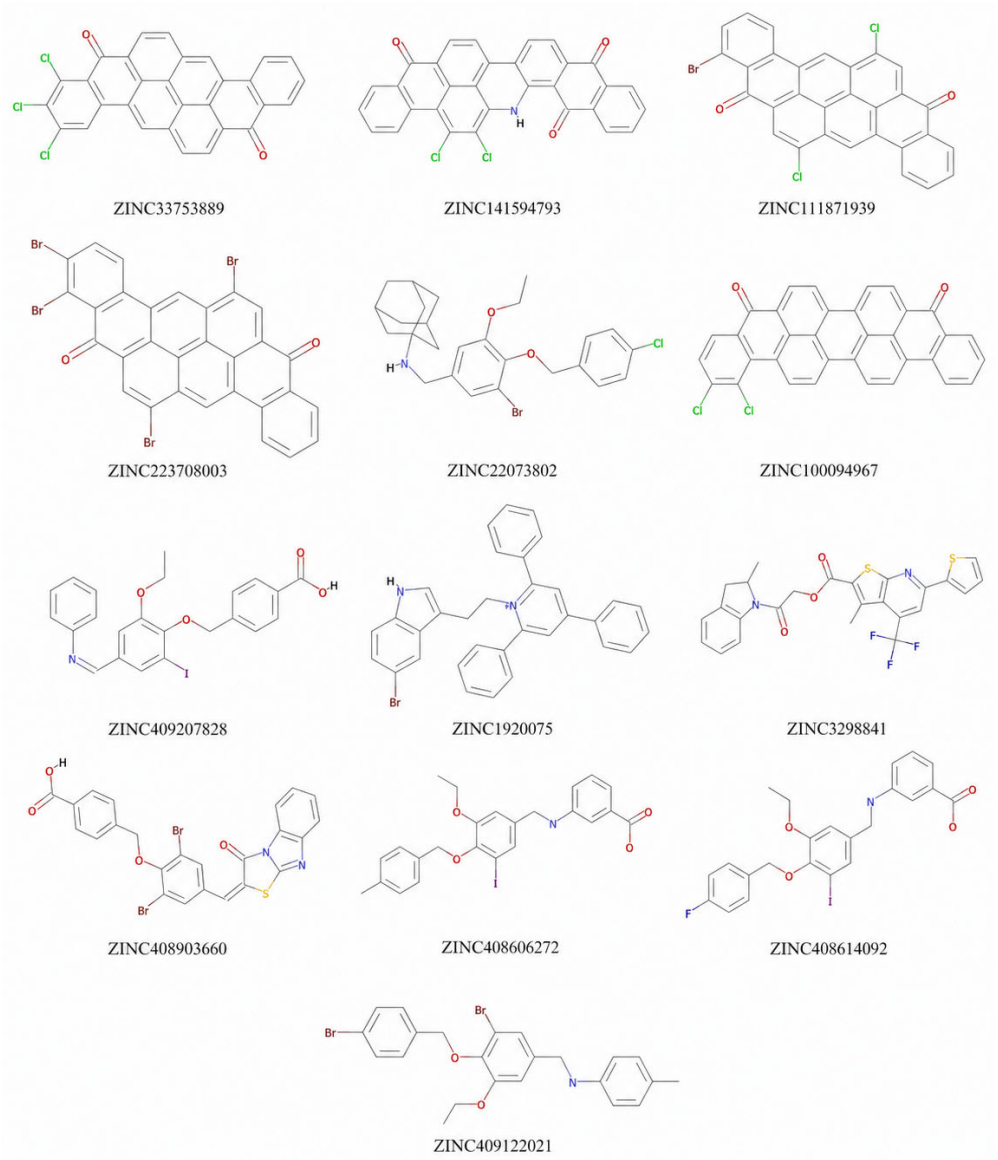


Figure 2. Chemical structures of the top docking hits against *L. infantum* and *L. mexicana* CFA synthases. Molecule **1** (ZINC33753889) and molecule **2** (ZINC111871939) share the 8,16-pyranthrenedione scaffold.

ADMET profiling of the top hits against L. infantum and L. mexicana CFA synthases (Table 3; SwissADME [23]) showed that the series is largely free of PAINS [24] (only ZINC141594793 was flagged) and carries few Brenk alerts [25]. As expected for a lipophilic pocket, all thirteen compounds are strongly lipophilic (XLOGP3 5.2–10.1, median 8.2), with low predicted gastrointestinal absorption in 9 of 13, so their development will depend on delivery strategies that are able to accommodate high lipophilicity. Then, 200 ns MD simulations confirmed stable complexes: ligand RMSD remained low (molecules **1** and **2**

below 0.1 nm) and protein RMSD increased only slightly while staying within a stable range (Figure 4); start-versus-final overlays (Figure 5) showed minimal drift. MM-PBSA binding energies (Table 4) were favorable across all systems (−140 to −191 kJ/mol), reaching −168 to −191 kJ/mol in the parasite enzymes, omitting configurational entropy intended for relative comparison. Energetic decomposition reveals that binding across all systems is predominantly driven by van der Waals interactions, consistent with the extensive aromatic core of the pyranthrenedione scaffold. Together, the cross-affinity, conserved-site occupancy and stability of the complex support the idea that pyrantridiones are examples of validated starting points, rather than definitive candidates.

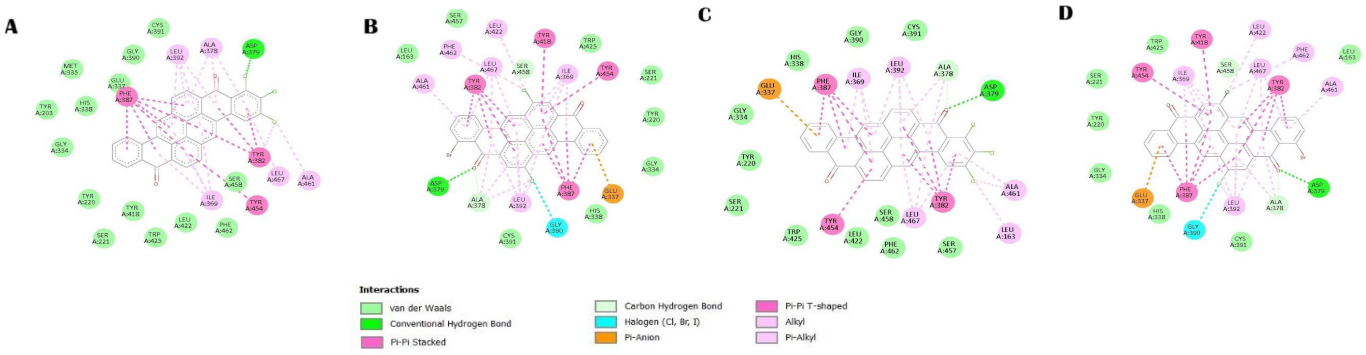


Figure 3. Key binding interactions of molecules **1** and **2** with *Leishmania* CFA synthases. (**A**) Molecule **1** with *L. infantum* CFA synthase. (**B**) Molecule **2** with *L. infantum* CFA synthase. (**C**) Molecule **1** with *L. mexicana* CFA synthase. (**D**) Molecule **2** with *L. mexicana* CFA synthase.

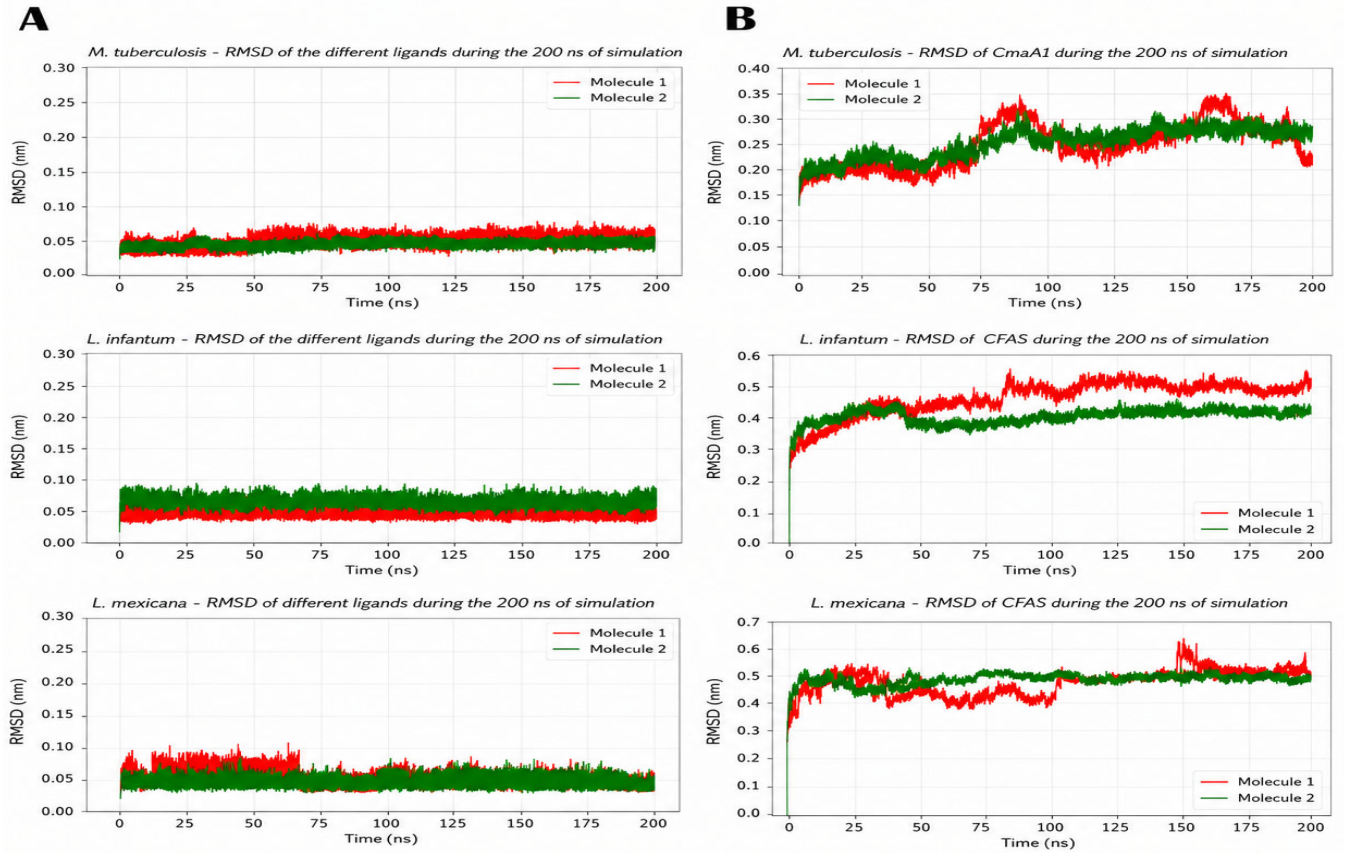


Figure 4. RMSD of ligands and targets in each system during the 200 ns trajectory. (**A**) Ligand RMSD. (**B**) Target RMSD.

Table 3. Drug-likeness and medicinal-chemistry alert profile of the top hits (SwissADME). PAINS/Brenk: number of alerts; lead-likeness: rule violations; synthetic accessibility: 1 (easy)−10 (hard).

ZINC20 ID	MW (g/mol)	XLOGP3	GI abs.	PAINS	Brenk	Lead viol.	Synth.
ZINC33753889 (1)	509.78	9.19	Low	0	2	2	3.43
ZINC141594793	518.35	9.51	Low	1	2	2	3.07
ZINC111871939 (2)	554.23	9.25	Low	0	1	2	3.47
ZINC223708003	722.02	10.07	Low	0	1	2	3.52
ZINC22073802	504.89	7.09	Low	0	0	3	5.41
ZINC100094967	525.38	9.81	Low	0	2	2	3.64
ZINC409207828	501.31	5.20	High	0	2	3	3.37
ZINC1920075	530.48	8.64	Low	0	1	2	3.44
ZINC3298841	516.56	6.57	Low	0	0	2	4.20
ZINC408903660	586.25	8.18	High	0	0	2	3.52
ZINC408606272	517.36	5.74	High	0	1	3	3.15
ZINC408614092	521.32	5.48	High	0	1	3	3.07
ZINC409122021	505.24	6.95	Low	0	0	3	2.92

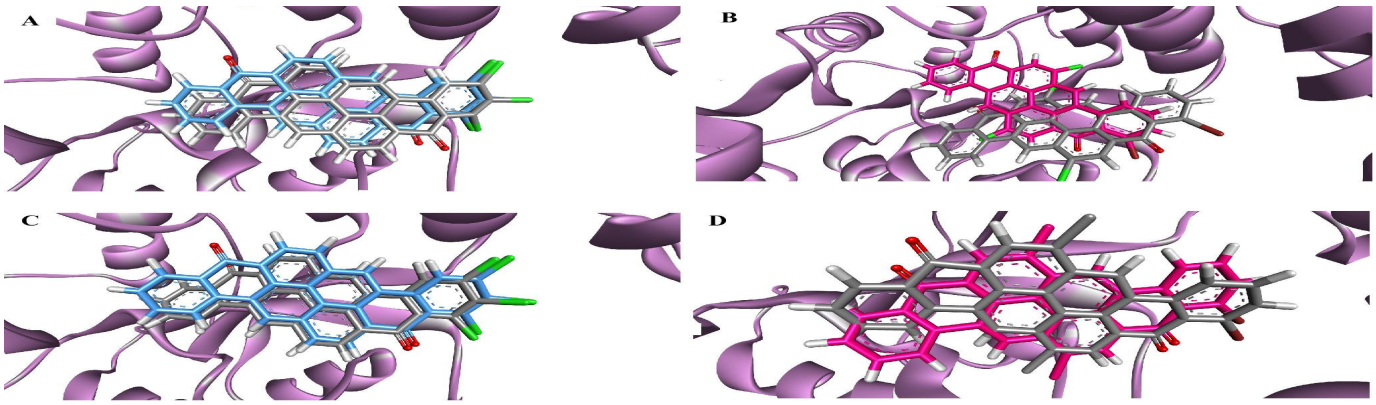


Figure 5. Comparison of starting and final structures of molecule **1** (blue) and molecule **2** (pink) after 200 ns; colored structures correspond to the initial conformations. (**A**,**B**) molecules **1** and **2** with *L. infantum* CFA synthase and (**C**,**D**) molecules **1** and **2** with *L. mexicana* CFA synthase.

Table 4. MM-PBSA binding free energies (ΔG bind) and energetic components (kJ/mol), omitting conformational entropy, averaged over the 10–200 ns MD production trajectories.

Target	Molecule	vdW	Elec.	Polar	SASA	ΔG Bind.
M. tuberculosis CmaA1	1	−251.20	−10.74	108.15	−22.34	−176.12
	2	−216.23	2.53	93.05	−19.61	−140.26
L. infantum CFA synthase	1	−257.45	−25.35	125.67	−21.93	−179.07
	2	−262.59	−9.61	108.85	−23.21	−186.55
L. mexicana CFA synthase	1	−255.44	−38.00	148.44	−23.06	−168.06
	2	−266.16	−13.17	110.20	−21.99	−191.12

4. Conclusions

Comparison with CmaA1 indicates that *Leishmania* CFA synthases share its catalytic mechanism: the conserved Tyr33, Cys35, Gly137 and Glu140 [6] point to the same SAM-

dependent cyclopropanation, here acting on membrane phospholipids, a modification that governs membrane composition, cell shape and acid-stress resistance and, though dispensable for axenic growth, required for full virulence in vivo [4,5]. Because this chemistry has no human counterpart and the pocket is conserved family-wide, the central proposal of this work is not a single chemotype but the CFA synthase family as a parasite-selective target class, and a possible basis for multi-target intervention. The screening on CmaA1 shows that the pocket is tractable and yields validated starting points; the pyranthrenedione hits are examples, not final candidates. Their high lipophilicity will require delivery strategies such as solid lipid nanoparticles [26,27]. The two species modeled span both clinical forms and thus two delivery scenarios: visceral disease (*L. infantum*) demands systemic exposure, whereas cutaneous lesions caused by *L. mexicana* allow topical or intralesional treatment [28], where low gastrointestinal absorption stops being limiting, though XLOGP3 above five still favors retention in the stratum corneum over partitioning into the dermal macrophages that host the parasite, so lipid vehicles [27] remain necessary.

Author Contributions: Conceptualization, J.D.G.; methodology, J.D.G., J.R.M. and M.L.; software, J.D.G., J.R.M. and M.L.; validation, J.D.G., J.R.M. and M.L.; formal analysis, J.R.M. and M.L.; investigation, J.D.G.; data curation, J.D.G.; writing—original draft preparation, J.D.G.; writing—review and editing, J.R.M. and M.L.; visualization, J.D.G., J.R.M. and M.L.; supervision, J.R.M. and M.L. All authors have read and agreed to the published version of the manuscript.

Funding: This research received no external funding.

Institutional Review Board Statement: Not applicable.

Informed Consent Statement: Not applicable.

Data Availability Statement: The raw data supporting the conclusions of this article will be made available by the authors upon request.

Acknowledgments: During the preparation of this manuscript, the authors used Claude Opus 5 (Anthropic) for the purposes of improving the language of the text. The authors have reviewed and edited the output and take full responsibility for the content of this publication.

Conflicts of Interest: The authors declare no conflicts of interest.

References

1. Cronan, J.E.; Luk, T. Advances in the Structural Biology, Mechanism, and Physiology of Cyclopropane Fatty Acid Modifications of Bacterial Membranes. *Microbiol. Mol. Biol. Rev.* **2022**, *86*, e00013-22. [CrossRef] [PubMed]
2. Yan, W.; Zheng, Y.; Dou, C.; Zhang, G.; Arnaout, T.; Cheng, W. The pathogenic mechanism of *Mycobacterium tuberculosis*: Implication for new drug development. *Mol. Biomed.* **2022**, *3*, 48. [CrossRef] [PubMed]
3. Diab, A.; Dickerson, H.; Al Musaimi, O. Targeting the Heart of *Mycobacterium*: Advances in Anti-Tubercular Agents Disrupting Cell Wall Biosynthesis. *Pharmaceuticals* **2025**, *18*, 70. [CrossRef] [PubMed]
4. Oyola, S.O.; Evans, K.J.; Smith, T.K.; Smith, B.A.; Hilley, J.D.; Mottram, J.C.; Smith, D.F. Functional Analysis of *Leishmania* Cyclopropane Fatty Acid Synthetase. *PLoS ONE* **2012**, *7*, e51300. [CrossRef] [PubMed]
5. Xu, W.; Mukherjee, S.; Ning, Y.; Hsu, F.F.; Zhang, K. Cyclopropane fatty acid synthesis affects cell shape and acid resistance in *Leishmania mexicana*. *Int. J. Parasitol.* **2018**, *48*, 245–256. [CrossRef] [PubMed]
6. Huang, C.C.; Smith, C.; Glickman, M.S.; Jacobs, W.R.; Sacchettini, J.C. Crystal structures of mycolic acid cyclopropane synthases from *Mycobacterium tuberculosis*. *J. Biol. Chem.* **2002**, *277*, 11559–11569. [CrossRef] [PubMed]
7. Hari, S.B.; Grant, R.A.; Sauer, R.T. Structural and Functional Analysis of *E. coli* Cyclopropane Fatty Acid Synthase. *Structure* **2018**, *26*, 1251–1258. [CrossRef] [PubMed]
8. Ma, Y.; Pan, C.; Wang, Q. Crystal structure of bacterial cyclopropane-fatty-acyl-phospholipid synthase with phospholipid. *J. Biochem.* **2019**, *166*, 139–147. [CrossRef] [PubMed]
9. Irwin, J.J.; Tang, K.G.; Young, J.; Dandarchuluun, C.; Wong, B.R.; Khurelbaatar, M.; Sayle, R.A. ZINC20-A Free Ultralarge-Scale Chemical Database for Ligand Discovery. *J. Chem. Inf. Model.* **2020**, *60*, 6065–6073. [CrossRef] [PubMed]

10. Hawkins, P.C.D.; Skillman, A.G.; Warren, G.L.; Ellingson, B.A.; Stahl, M.T. Conformer Generation with OMEGA. *J. Chem. Inf. Model.* **2010**, *50*, 572–584. [CrossRef] [PubMed]
11. Bertoni, D.; Tsenkov, M.; Magana, P.; Nair, S.; Pidruchna, I.; Afonso, M.Q.L.; Midlik, A.; Paramval, U.; Lawal, D.; Tanweer, A.; et al. AlphaFold Protein Structure Database 2025: A redesigned interface and updated structural coverage. *Nucleic Acids Res.* **2026**, *54*, D358–D362. [CrossRef] [PubMed]
12. Corpet, F. Multiple sequence alignment with hierarchical clustering. *Nucleic Acids Res.* **1988**, *16*, 10881–10890. [CrossRef] [PubMed]
13. Gouet, P.; Robert, X.; Courcelle, E. ESPript/ENDscript: Extracting and rendering sequence and 3D information from atomic structures of proteins. *Nucleic Acids Res.* **2003**, *31*, 3320–3323. [CrossRef] [PubMed]
14. Pettersen, E.F.; Goddard, T.D.; Huang, C.C.; Couch, G.S.; Greenblatt, D.M.; Meng, E.C.; Ferrin, T.E. UCSF Chimera-A visualization system for exploratory research and analysis. *J. Comput. Chem.* **2004**, *25*, 1605–1612. [CrossRef] [PubMed]
15. Dassault Systèmes. *BIOVIA Discovery Studio*, Version 25.1.0.24284; Dassault Systèmes: San Diego, CA, USA, 2025.
16. McGann, M. FRED and HYBRID docking performance on standardized datasets. *J. Comput. Aided Mol. Des.* **2012**, *26*, 897–906. [CrossRef] [PubMed]
17. Abraham, M.J.; Murtola, T.; Schulz, R.; Páll, S.; Smith, J.C.; Hess, B.; Lindahl, E. GROMACS: High performance molecular simulations through multi-level parallelism from laptops to supercomputers. *SoftwareX* **2015**, *1*, 19–25. [CrossRef]
18. Sousa da Silva, W.S.; Vranken, W.F. ACPYPE-AnteChamber PYthon Parser interfacE. *BMC Res. Notes* **2012**, *5*, 367. [CrossRef] [PubMed]
19. O'Boyle, N.M.; Banck, M.; James, C.A.; Morley, C.; Vandermeersch, T.; Hutchison, G.R. Open Babel: An open chemical toolbox. *J. Cheminform.* **2011**, *3*, 33. [CrossRef] [PubMed]
20. Kumari, R.; Kumar, R.; Open Source Drug Discovery Consortium; Lynn, A. g_mmpbsa—A GROMACS Tool for High-Throughput MM-PBSA Calculations. *J. Chem. Inf. Model.* **2014**, *54*, 1951–1962. [CrossRef] [PubMed]
21. Liao, R.; Georgieva, P.; Yu, J.; Himo, F. Mechanism of Mycolic Acid Cyclopropane Synthase: A Theoretical Study. *Biochemistry* **2011**, *50*, 1505–1513. [CrossRef] [PubMed]
22. Choudhury, C.; Priyakumar, U.D.; Sastry, G.N. Molecular dynamics investigation of the active site dynamics of mycobacterial cyclopropane synthase during various stages of the cyclopropanation process. *J. Struct. Biol.* **2014**, *187*, 38–48. [CrossRef] [PubMed]
23. Daina, A.; Michielin, O.; Zoete, V. SwissADME: A free web tool to evaluate pharmacokinetics, drug-likeness and medicinal chemistry friendliness of small molecules. *Sci. Rep.* **2017**, *7*, 42717. [CrossRef] [PubMed]
24. Baell, J.B.; Holloway, G.A. New Substructure Filters for Removal of Pan Assay Interference Compounds (PAINS). *J. Med. Chem.* **2010**, *53*, 2719–2740. [CrossRef] [PubMed]
25. Brenk, R.; Schipani, A.; James, D.; Krasowski, A.; Gilbert, I.H.; Frearson, J.; Wyatt, P.G. Lessons learnt from assembling screening libraries for drug discovery for neglected diseases. *ChemMedChem* **2008**, *3*, 435–444. [CrossRef] [PubMed]
26. Duan, Y.; Dhar, A.; Patel, C.; Khimani, M.; Neogi, S.; Sharma, P.; Vekariya, R.L. A brief review on solid lipid nanoparticles. *RSC Adv.* **2020**, *10*, 26777–26791. [CrossRef] [PubMed]
27. Santamaria-Aguirre, J.; Jacho, D.; Mendez, M.A.; Poveda, A.; Carrión, J.; Fanarraga, M.L. Solid Lipid Nanoparticles Enhancing the Leishmanicidal Activity of Delamanid. *Pharmaceutics* **2024**, *16*, 41. [CrossRef] [PubMed]
28. Azim, M.; Khan, S.A.; Ullah, S.; Anjum, S.I. Therapeutic advances in the topical treatment of cutaneous leishmaniasis: A review. *PLoS Negl. Trop. Dis.* **2021**, *15*, e0009099. [CrossRef] [PubMed]

Disclaimer/Publisher's Note: The statements, opinions and data contained in all publications are solely those of the individual author(s) and contributor(s) and not of MDPI and/or the editor(s). MDPI and/or the editor(s) disclaim responsibility for any injury to people or property resulting from any ideas, methods, instructions or products referred to in the content.